Consequences of violation of frozen-in-flux: Evidence from OpenGGCM simulations

B. Hu,[1] R. A. Wolf,[1] F. R. Toffoletto,[1] J. Yang,[1] and J. Raeder[2]

Received 18 March 2011; revised 12 May 2011; accepted 6 June 2011; published 30 June 2011.

[1] It is widely believed that during a substorm, plasma instabilities occur before the onset of magnetic reconnection, signaling the end of the growth phase. Despite many years of effort, however, the details of how the instability and the onset of reconnection develop from closed field line configuration with finite normal magnetic field are not well understood. In this paper, we study an idealized simulation of a substorm that occurred on 23 March 2007, based on the Open Geospace General Circulation Model (OpenGGCM). Our analysis emphasizes the time development of the distribution of the entropy parameter and its convective time derivative, which should be zero in ideal MHD. In the late growth phase, the simulation exhibits, over a range of local times, a systematic violation of conservation of entropy that corresponds to what is called "antidiffusion." Out of this background, a more localized disturbance develops in a region of high magnetic stretching, resulting in formation of a strong reduction of entropy (bubble) earthward of a local enhancement (blob). The process is accelerated when the current density exceeds a threshold for triggering an explicit resistivity in the code. The bubble moves earthward and the blob tailward, which leads to a reduction of the normal magnetic field and a thinning of the current sheet between them, making the magnetospheric configuration more conducive to tearing and other instabilities (we do not address specifically which instability has occurred). This positive feedback gives rise to increased violation of the perfect conductivity relation and eventually reconnection.

Citation: Hu, B., R. A. Wolf, F. R. Toffoletto, J. Yang, and J. Raeder (2011), Consequences of violation of frozen-in-flux: Evidence from OpenGGCM simulations, *J. Geophys. Res.*, *116*, A06223, doi:10.1029/2011JA016667.

1. Introduction

[2] Many authors have suggested that instabilities occur before the onset of substorm expansion phase that may change the magnetotail to a more favorable configuration for magnetic reconnection (see reviews by *Lui* [2004], *Cheng* [2004], and *Pritchett* [2007]). However, the details on how reconnection arises from an initial closed field line configuration with finite normal magnetic fields are a matter of longstanding controversy, as reviewed briefly by *Sitnov and Schindler* [2010]. (In this paper, we use *Vasyliunas*' [1975] definition of reconnection in terms of plasma flow across a separatrix between field lines of different topology. However, as the separatrix may not be easily identifiable until lobe reconnection starts, we will say specifically that reconnection has occurred if and only if the magnetic field crosses the center of the cross-tail current sheet in both directions. Thus reconnection, in our definition, is required to produce the helical field lines that can occur in the plasma sheet in the presence of finite B_y.)

[3] Recently, *Yang et al.* [2011] shed light on initiation of reconnection starting from a closed field line plasma sheet configuration by using the RCM-E (Rice Convection Model-Equilibrium) to simulate an idealized substorm growth phase in which they imposed up a local reduction of $pV^{5/3}$ (where p is the pressure and V is the flux tube volume $\int ds/B$) forming a bubble just earthward of a local enhancement of $pV^{5/3}$ (blob) at the end of a substorm growth phase [*Zhang et al.*, 2008; *Wolf et al.*, 2009]. The bubble and blob were assumed to be created by unspecified mechanisms that violated the local frozen-in-flux condition. *Yang et al.* [2011] found that the bubble moves earthward and the blob surges tailward. In the region between them, the current sheet thins and the normal magnetic field decreases. Because of that, Yang et al. suggested that the creation of a bubble/blob pair in the RCM-E simulation leads to a magnetospheric configuration that is more conducive to tearing. However, because of the slow flow and quasi-static equilibria assumptions used in the RCM-E [*Wolf*, 1983], the simulations used by *Yang et al.* [2011] have two limitations: (1) the inertial term in the momentum equation is neglected and (2) the process of reconnection is not represented in the model. Here we present MHD

[1]Department of Physics and Astronomy, William Marsh Rice University, Houston, Texas, USA.
[2]Space Science Center, University of New Hampshire, Durham, New Hampshire, USA.

0148-0227/11/2011JA016667

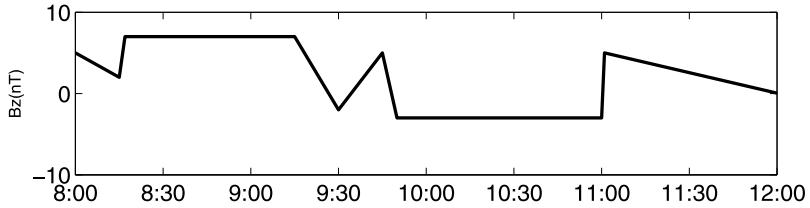

Figure 1. IMF B_z input for the OpenGGCM simulation (shifted to sunward simulation boundary).

simulations that have neither of these limitations and so add a useful additional computational test of the ideas presented by *Yang et al.* [2011].

[4] As in the *Yang et al.* [2011] study, the MHD code does not specifically model any potential non-MHD microscale mechanisms that lead to the violation of frozen-in-flux. In the Open Geospace General Circulation Model (OpenGGCM) MHD code, the frozen-in-flux condition can be locally violated in one of two ways. The first is numerical diffusion, in which finite grid discretization inevitably gives rise to errors in the second-order derivatives of the magnetic field, creating numerical dissipation. The second mechanism that operates in the OpenGGCM takes the form of a built-in explicit anomalous resistivity which is triggered when the normalized current density exceeds a specified threshold [*Raeder et al.*, 1998]. The anomalous diffusion caused by the anomalous resistivity is on the scale of grid cell and is usually large when it is activated; however observations suggest even stronger diffusion in the tail [e.g., *Cattell*, 1996]. In either case, either mechanism might be expected to produce field line slippage in the region with numerical or anomalous resistivity, resulting in plasma transport from one flux tube to the other, violating the frozen-in-flux condition, and creating a bubble and a blob [*Yang et al.*, 2011, Figure 1].

[5] In this paper, we will present detailed results from an idealized OpenGGCM MHD simulation, based on a substorm event that occurred on 23 March 2007—an event that has been studied by *Raeder et al.* [2008], *Zhu et al.* [2009], *Hu et al.* [2010], and *Raeder et al.* [2010] using realistic solar wind and IMF input. We show that a bubble-blob pair forms naturally in the simulation and discuss the reason for their formation. The results of this paper, along with the RCM-E results [*Yang et al.*, 2011], further support the idea that the bubble-blob mechanism contributes importantly to the start of reconnection near the onset of the substorm expansion phase.

2. The OpenGGCM Simulation

[6] OpenGGCM is a large-scale model of the Earth's magnetosphere which is described in detail by *Raeder* [2003] and *Raeder et al.* [2008]. For the runs presented here, we used a grid resolution, in the x, y and z directions, of 630 × 300 × 200 with the smallest grid spacing at ~0.15 R_E. The CTIM module [*Fuller-Rowell et al.*, 1996] in OpenGGCM was used for ionospheric conductance calculations. The solar wind inputs for the OpenGGCM were smoothed and simplified versions of the actual data from the WIND satellite (at ~198 R_E sunward) but with B_x, B_y, V_y, and V_z set to zero to make the results easier to visualize. The simplified time variation of the interplanetary magnetic field (IMF) B_z component at the sunward boundary is shown in Figure 1. The solar wind density is constant at 15 particles/cc, until it jumps to 20 particles/cc at 11:00. The solar wind velocity V_x is held constant at 300 km/s. The dipole tilt is set to zero for simplicity.

[7] This paper focuses on analyzing MHD results using an entropy parameter similar to $pV^{5/3}$. Two technical points require discussion.

[8] In simulations with the RCM-E, which assumes a series of configurations that are in force equilibrium, *Yang et al.* [2011] focused on the parameter $pV^{5/3}$, which is constant in adiabatic expansion or compression of an ideal monatomic gas. In full MHD, with inertial terms present, pressure is not constant along field lines, and the generalization of $pV^{5/3}$ is $S^{5/3}$, where

$$S = \int p^{3/5} ds/B = \int \left(\frac{p^{3/5}}{\rho}\right) \frac{\rho\, ds}{B} \tag{1}$$

[*Birn et al.*, 2009]. Under conditions of frozen-in-flux, the quantity $\rho ds/B$, which is an element of mass along the flux tube, should be conserved as the element moves. The parameter $p^{3/5}/\rho$ is equal to $(1/C)\exp(\sigma/R)$, where C and R are constants, and σ is entropy per unit mass defined as $R\ln(Cp^{3/5}/\rho)$ [*Birn et al.*, 2009]. Thus $p^{3/5}/\rho$ is conserved as a mass element moves in ideal MHD, because entropy is conserved. Of course, $S^{5/3}$ is equal to $pV^{5/3}$ in the special case where pressure is constant along a field line, and we will focus on $S^{5/3}$ in our MHD-based study.

[9] In ideal MHD,

$$\frac{DS^{5/3}}{Dt} = \frac{\partial S^{5/3}}{\partial t} + \mathbf{v}\cdot\nabla S^{5/3} = 0 \tag{2}$$

where $\mathbf{v}$ is the flow velocity. When the frozen-in-flux condition is violated, we will still use flow velocity to calculate $\frac{DS^{5/3}}{Dt}$ as a diagnostic parameter; in this case $\frac{DS^{5/3}}{Dt}$ would be nonzero. Since $S^{5/3}$ is constant along a field line we can display it or $DS^{5/3}/Dt$ on any surface that cuts all of the field lines considered. It is easiest to visualize equation (2) if the surface is defined such that the gradient is parallel to the surface, so that we can consider only the velocities on that surface. For the present runs, the dipole is untilted, and the boundary conditions have north-south symmetry, so the equatorial magnetic field should be exactly perpendicular to the equatorial plane, and $\nabla S^{5/3}$ should be in the plane. However, this symmetry condition is not built into the numerical procedure and is consequently not exactly satisfied; that is, in certain regions the equatorial V_z is

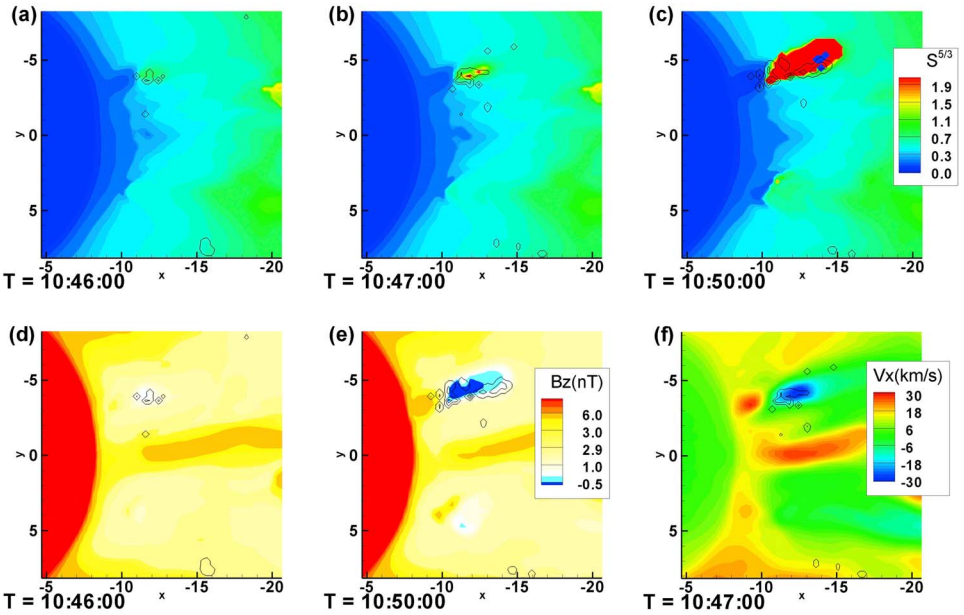

Figure 2. (a–c) Equatorial values of $S^{5/3}$ for times 10:46, 10:47, and 10:50. (d and e) B_z on the equatorial plane for 10:46 and 10:50. (f) Flow velocity in the x direction for 10:47. The black closed loops on the $S^{5/3}$ plots indicate where the anomalous resistivity is nonzero.

not exactly zero. To account for the nonzero V_z, in the calculation of $\frac{DS^{5/3}}{Dt}$, we made certain corrections to **v** in equation (2), as described in Appendix A. The effect of the correction is very small for regions of interest and is only visible for a limited region ($x < -16$ R_E, $4 < y < 6$).

2.1. Bubble-Blob Pair and Numerical Accuracy Issues

[10] In the simulation, the IMF turns southward at ~10:00 UT and turns northward at ~11:00 UT at the sunward simulation boundary. In this paper, we focus on the period near the end the growth phase 10:35–10:50 UT. Before 10:30 UT, the MHD simulation shows a classic growth phase picture with field line stretching. Figures 2a–2c show plots of $S^{5/3}$ in the $z = 0$ plane at times 10:46, 10:47, 10:50. Figures 2d and 2e show two snapshots of the z component of the equatorial magnetic field at 10:46 and 10:50. Note that the blue areas represent $B_z < 0$, which indicates that reconnection has occurred. Areas with negative equatorial B_z but positive values for $S^{5/3}$ indicate presence of helical field lines. (f) shows the flow velocity in the x direction.

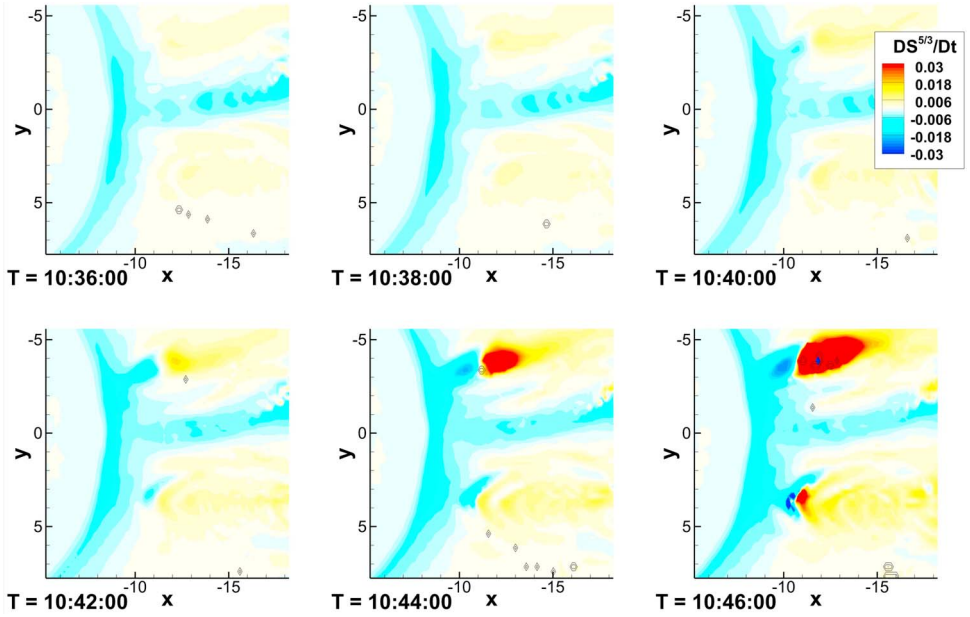

Figure 3. Equatorial $DS^{5/3}/Dt$ values for six different times: 10:36, 10:38, 10:40, 10:42, 10:44, and 10:46.

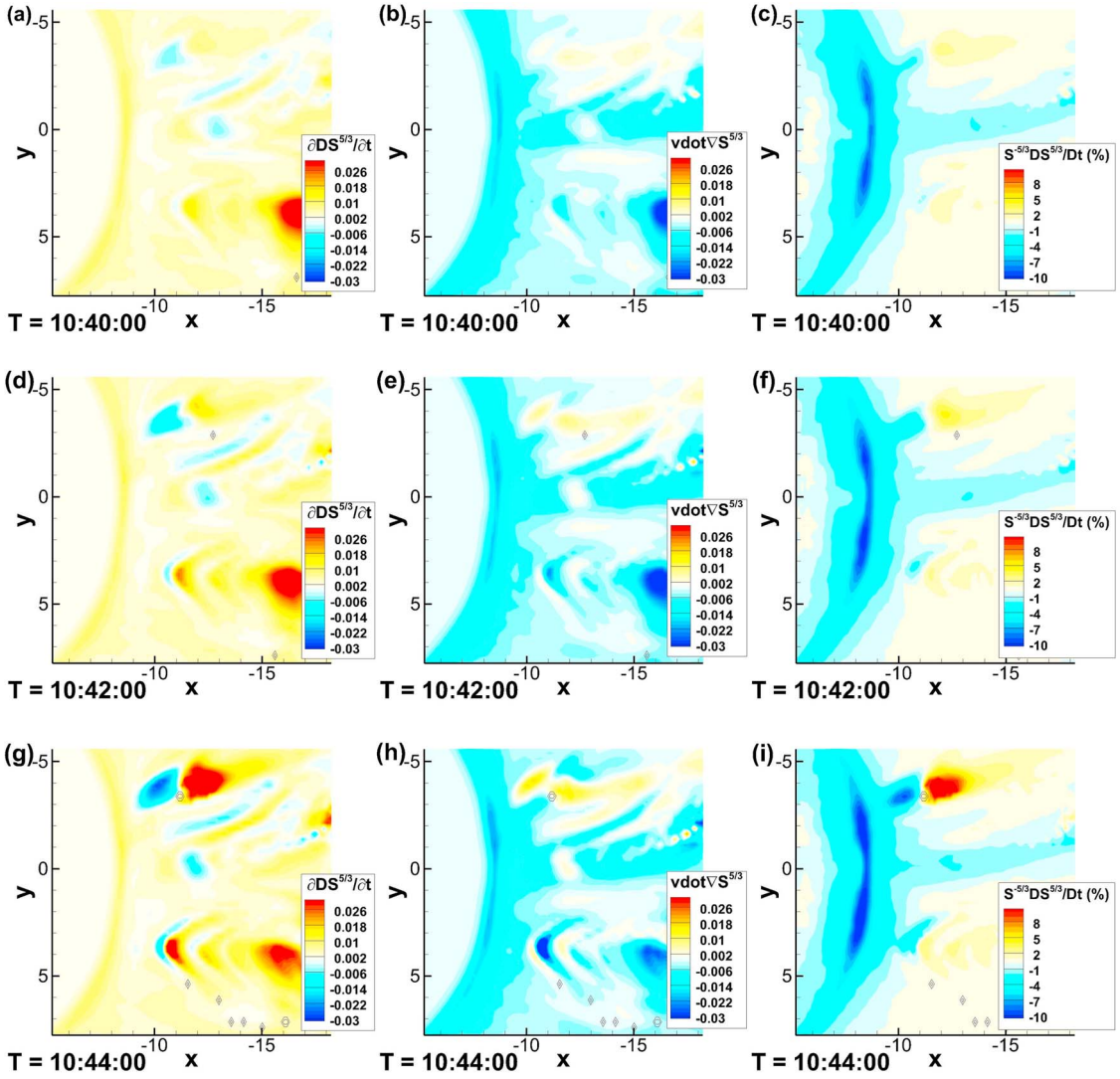

Figure 4. Equatorial values of $\partial S^{5/3}/\partial t$, $(\mathbf{v}_2 \cdot \nabla)S^{5/3}$, and $S^{-5/3}\,\frac{DS^{5/3}}{Dt}$ (per minute) for 10:40, 10:42, and 10:44.

The black closed loops on the $S^{5/3}$ plots indicate where the anomalous resistivity is nonzero.

[11] One clear feature of Figures 2d and 2e is a channel of earthward flow near local midnight, and Figures 2a and 2b indicate a slight reduction of $S^{5/3}$ in that region. This feature is reminiscent of the flow channels suggested by *Sergeev and Lennartsson* [1988]. A more interesting feature is a bubble-blob pair that develops east of local midnight, which we will discuss in detail. (A similar feature develops before midnight a few minutes later, but our discussion will focus on the postmidnight feature.)

[12] Figure 3 shows $DS^{5/3}/Dt$ for six times during the simulation. If the code were solving the ideal MHD equations exactly, then $DS^{5/3}/Dt$ would be zero everywhere except inside the closed black curves, where the resistivity is explicitly set equal to positive values. Obviously, that is not the situation, and most of the nonzero values shown in Figure 3 are a result of numerical diffusion. To understand better what is happening in the code at 10:40, we display separately in Figures 4a and 4b the $\partial S^{5/3}/\partial t$ and $\mathbf{v} \cdot \nabla S^{5/3}$ terms in equation (2), respectively. Figure 4c shows $S^{-5/3}\,\frac{DS^{5/3}}{Dt}$, which is the percentage change of $S^{5/3}$ per minute. In the injection channel near midnight, $|\mathbf{v} \cdot \nabla S^{5/3}| \gg |\partial S^{5/3}/\partial t|$, presumably because of the relatively large flow velocities and the tailward gradient of $S^{5/3}$. The two terms in (5) do not balance because of the tendency of MHD codes to numerically diffuse pressure from the high-pressure region in the inner plasma sheet toward the lower-pressure region further out. However, *Lee et al.* [1995] suggested the existence of a physical mechanism that acts in the same direction.

[13] The most interesting feature in Figures 3 and 4 is in the region centered about (−11, −3), where Figure 2 indicates the formation of a bubble and a blob. In this feature, which is narrow in local time, there is a region where $\partial S^{5/3}/\partial t$ and $D^{5/3}/Dt$ are both negative, indicating the creation of a bubble through violation of the adiabatic condition. Tailward of the bubble is a region where $\partial S^{5/3}/\partial t$ and $D^{5/3}/Dt$ are both positive, indicating the creation of a blob. In the bubble/blob region the $\partial S^{5/3}/\partial t$ term dominates in $DS^{5/3}/Dt$, as shown in Figure 4.

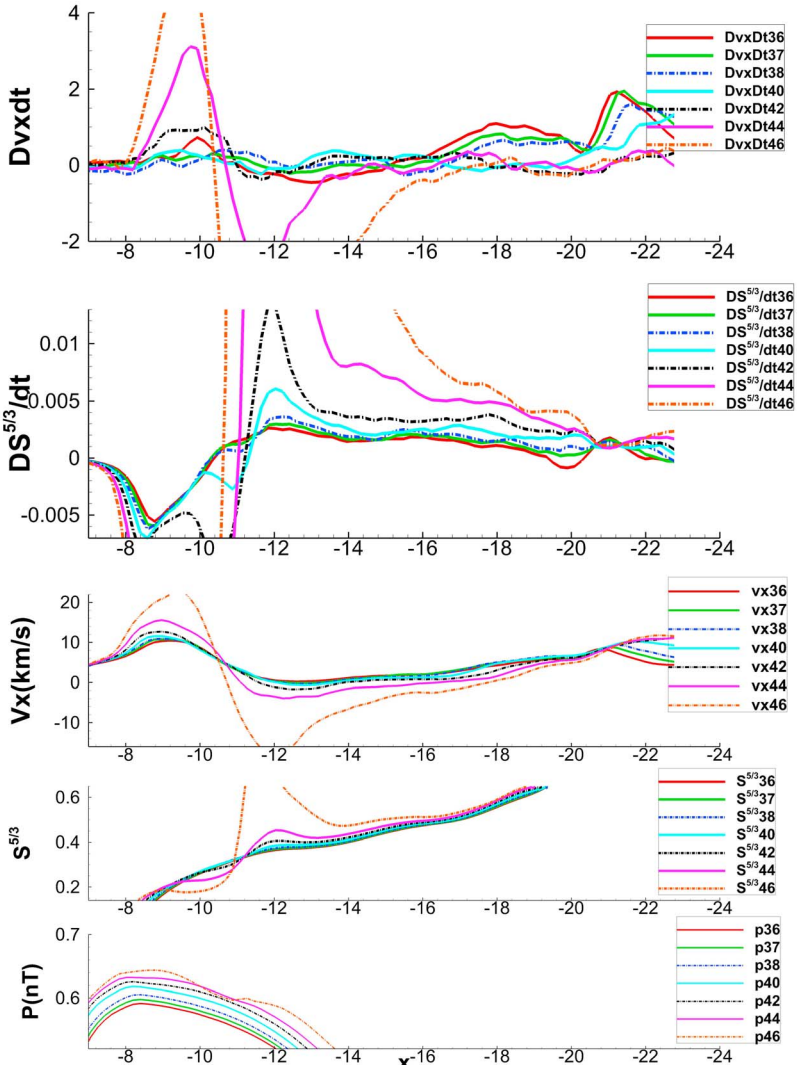

Figure 5. Dv_x/Dt, $DS^{5/3}/Dt$, v_x, $S^{5/3}$, and pressure along the centerline of the bubble-blob pair versus x in the equatorial plane, for the times indicated.

[14] Figures 5 and 6 show the development of the bubble-blob pair in more quantitative detail. They show the variation of several physical parameters along the approximate centerline of the bubble/blob pair, which we estimate as

$$y = \frac{x}{3} - 0.24$$

The two interesting features are as follows.

[15] 1. The situation before 10:37 is characterized by $DS^{5/3}/Dt < 0$ centered at about $x = -9$ and $DS^{5/3}/Dt > 0$ centered around $x = -11$ R_E. Those features, which cover a fairly wide range of local time in the postmidnight sector, are of numerical origin in the code and represent numerical anti-diffusion in S. It is called "antidiffusion" because the gradient of S usually points tailward and this diffusion in pressure makes the gradient of S stronger. These features grow in time, slowly but steadily. Figure 6a indicates that an increasingly deep magnetic field minimum forms around $x = -11$ R_E. It represents essentially the antidiffusion behavior predicted by *Lee et al.* [1995]. The Dv_x/Dt plot in Figure 5 indicates that there is very little acceleration associated with this antidiffusion. At 10:46, although the bubble and blob pair is well formed, the earthward and tailward flow is not strong, with a peak x velocity at ~20 km/s. The diffusion in pressure is not noticeable until 10:46, as shown in Figure 5.

[16] 2. Beginning about 10:38, $DS^{5/3}/Dt$ begins to decrease at about x = −10.8 on the centerline, and that feature rapidly becomes sharp. $DS^{5/3}/Dt$ increases tailward of $x = -11.2$. Figure 3 indicates that this rapidly developing feature is quite narrow in local time. A bubble and blob form. Acceleration also builds up at approximately the same time—earthward in the bubble and tailward in the blob.

[17] The physical mechanism by which the bubble and blob could form in nature is illustrated in Figure 7. In the 2D stretched closed field line configuration shown in Figure 7a, suppose that the current density exceeds a threshold for generation of anomalous resistivity in the gray region. Then the electric field in the rest frame of the plasma is in the direction of the current (+y), and field line 2 slips earthward (x direction) through the plasma, reaching the configuration shown in Figure 7b. The magnetic field between lines 2 and

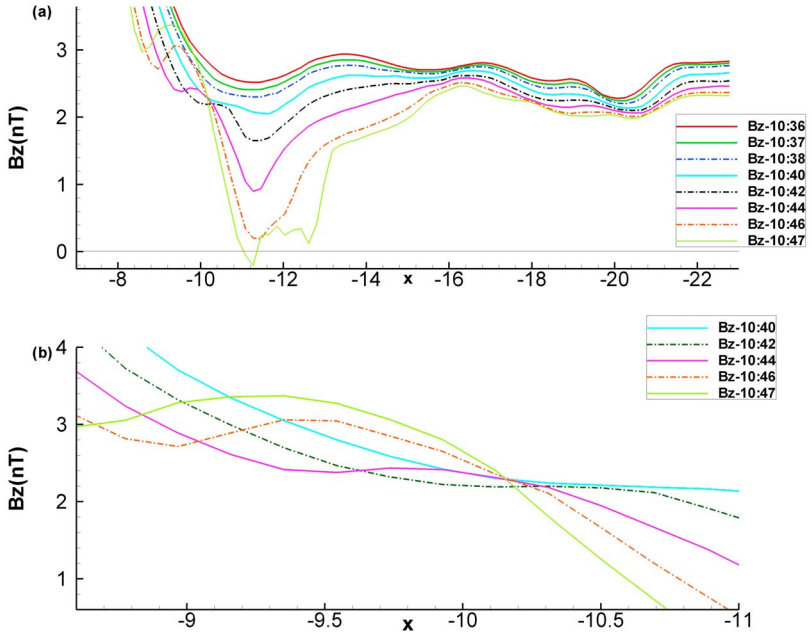

Figure 6. (a) B_z along the centerline of the bubble-blob pair versus x in the equatorial plane, for the times indicated. (b) Zoomed-in version of Figure 6a to show the bubble.

3 consequently strengthens, and the field between 1 and 2 weakens. The net force per unit volume can be written

$$\mathbf{f} = -\nabla p_{tot} + \frac{(\mathbf{B}\cdot\nabla)\mathbf{B}}{\mu_o} \tag{3}$$

where p_{tot} is the total pressure (particle + magnetic). If the region of slippage is thin in the y direction, as is the case in Figure 2, then p_{tot} in the slip region is approximately the same as in the adjacent background, which is assumed to be in equilibrium ($\mathbf{f} = 0$). The magnetic field in the bubble is stronger than in the background, and the same is true of the earthward tension force in the bubble. Therefore, the bubble feels a net earthward force. By the same kind of argument, the blob feels a tailward force. Note that in Figure 6, the B_z component in the bubble region is increasing for 10:46 and 10:47, despite the overall decreasing trend in B_z.

[18] One of the basic questions about how tearing can occur, starting from a configuration with finite magnetic field normal to the current sheet, is whether the same basic process that created a localized neutral sheet region from the $B_z > 0$ configuration is essentially the same as the mechanism that allows reconnection to proceed as in the classic reconnection geometry of Figure 7c. There is a resemblance between the situations in Figures 7b and 7c. In Figure 7b, strengthened tension force pulls the bubble on the earthward side toward the earth, and weakened tension force on the tailward side pulls the blob tailward. In Figure 7c there is earthward tension force on the earthward side of the neutral point, and tailward tension force on the tailward side. Both processes result from changes in the magnetic tension force.

2.2. The Role of Anomalous Resistivity

[19] In order to investigate the role of the anomalous resistivity in the formation of the bubble-blob pair, we have done two further runs, one that has the explicit resistivity completely turned off (Figure 8, top) and the other in which the explicit resistivity turned on until 10:00 (and turned off afterward) so that the system evolves to the exact same condition as in the original run at 10:00. This allows for easier comparison (Figure 4, middle).

[20] For the run without explicit resistivity, we still see the formation of the bubble and blob at the end of the growth phase, suggesting that numerical resistivity plays a role in their formation. These results suggest that a similar bubble/blob feature may also be reproduced by other global MHD models that have no explicit resistivity. However, the

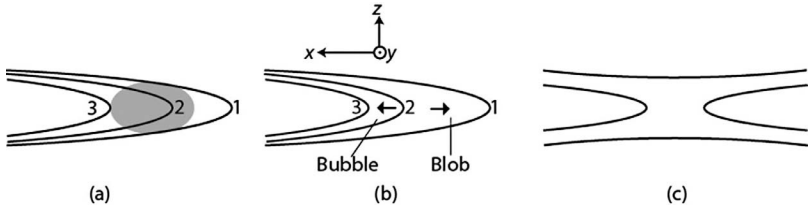

Figure 7. Illustration of the formation of bubble and blob due to region of anomalous resistivity and resulting acceleration (arrows).

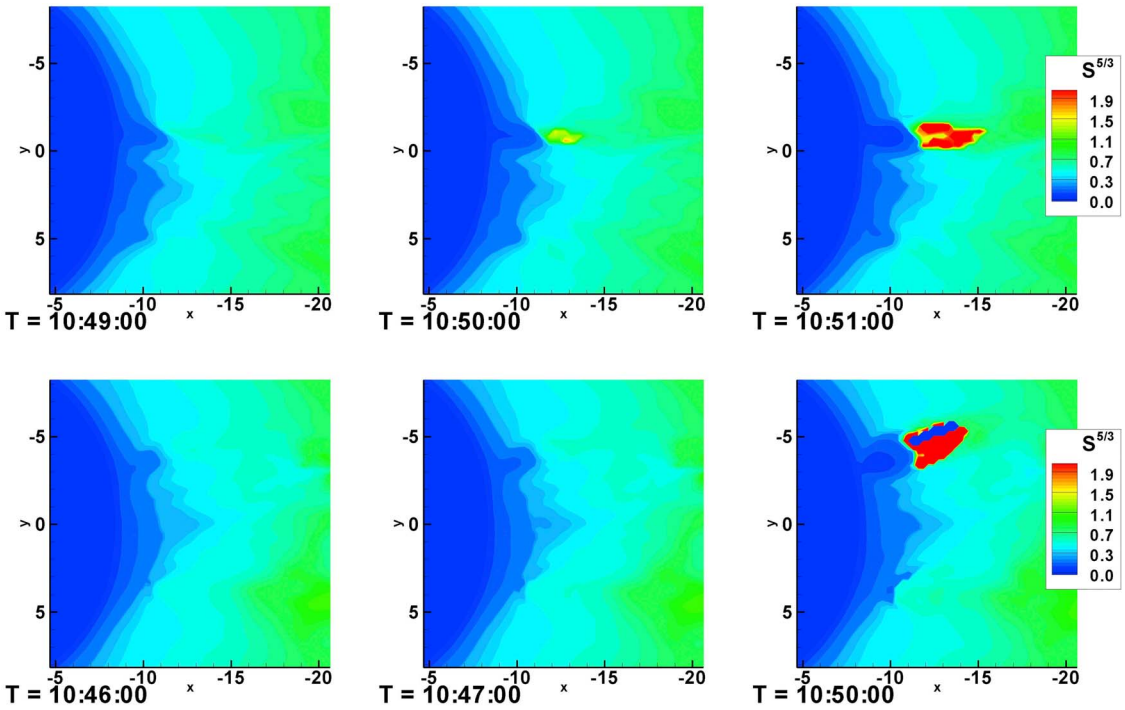

Figure 8. (top) $S^{5/3}$ on the equatorial plane for the run with zero explicit resistivity. (bottom) $S^{5/3}$ on the equatorial plane for the run with explicit resistivity on initially but turned off at 10:00.

anomalous resistivity does play an important role in the process. In the run with explicit resistivity turned off, the formation of the bubble and blob occurs later than in the run with resistivity turned on, so that the growth of the instability is slower. For the run with explicit resistivity turned off at 10:00, the blob also appears later and more weakly than the original run. That is, the field line slippage may begin due to numerical resistivity, creating a stretched configuration between a weak bubble and a weak blob, and this is followed by an increase in the current density within the stretched configuration, which in turn triggers the explicit resistivity, which helps the instability grow faster.

3. Discussion and Summary

[21] This paper has centered on the verification, in terms of a global MHD code, of the bubble-blob picture of how reconnection starts in a highly stretched inner plasma sheet, which is a central issue in the longstanding mystery of substorm onset. The physics of substorm onset has long been one of the leading questions of magnetospheric physics. However, it is still not known exactly why stress gradually builds up in the tail and then gets released suddenly. *Siscoe et al.* [2009] pointed out that, if we could answer that magnetospheric physics question, we might have an answer for the similar question for CMEs in the solar corona. In the paper by *Yang et al.* [2011], we proposed a partial answer to that question for the magnetosphere in terms of violation of frozen-in-flux in a highly stretched inner plasma sheet and consequent formation of a bubble and a blob, leading to reconnection. We have demonstrated that it is easy to identify the development of a bubble-blob pair in a global MHD simulation. The demonstration simply requires plots of the time sequence of V_x and S or its 5/3 power in the center of the current sheet. *Birn et al.* [2011] showed entropy reduction in the near tail using a similar entropy analysis in an MHD simulation. The reduction is found to occur near the onset of reconnection and prior to the onset of fast reconnection and that leads to bubbles surging into the inner magnetosphere.

[22] One significant aspect of this paper is the demonstration that $S^{5/3}$ can be a useful diagnostic for global MHD simulations, particularly for the plasma sheet. One advantage of using the parameter $S^{5/3}$ is that it reduces to the thermodynamic quantity $pV^{5/3}$ in the limit of force equilibrium; that parameter plays a key role in interchange processes, which are crucial to plasma–sheet dynamics. The parameter $S^{5/3}$ is useful for assessing the accuracy with which the code solves its differential equations and for visualizing the regions where physical violation of $S^{5/3}$ conservation is most important. An additional advantage of $S^{5/3}$ as a diagnostic is that it is a characteristic of an entire field line and so can be represented as a contour plot on the equatorial plane, for example.

[23] The *Yang et al.* [2011] paper confirmed the bubble-blob idea with the RCM-E, which has the limitations that it does not include inertial effects and cannot represent magnetic reconnection. The present paper is based on a global MHD simulation, which does include inertia and represents reconnection, but it does not include effects of transport by gradient/curvature drift. More importantly, global MHD models have significant numerical accuracy issues, particularly with regard to conservation of $S^{5/3}$ (Figure 4), which plays such an important role in plasma sheet dynamics. Conservation of the entropy parameter is violated in the

MHD code largely because of numerical dissipation. Thus the simulation results cannot shed light on the small-scale processes involved in real entropy nonconservation or on whether the dissipation processes that operate before reconnection starts are the same as those that sustain it, once it starts. At t = 10:47 and x = −11 R_E, the full z thickness half maximum for the y component of the current density is about 1 R_E. In contrast, the ion gyro radius in this region is ~1100 km and the ion inertia length ~100 km; thus the current sheet thickness is not yet close to the ion gyro radius. We can only hope that the numerical dissipation that occurs in regions where sharp gradients occur in the code mimic the effects of microscale physical dissipation. There is no numerical code that we can confidently apply to the inner plasma sheet. The best we can do is to use different codes, with different strengths and weaknesses, which is what we have done in testing the bubble-blob idea with both RCM-E and OpenGGCM.

[24] Comparison between OpenGGCM and the RCM-E simulations cannot easily separate the effects of inertia and gradient/curvature drifts, because it is very difficult to make the run setups the same in the two codes and because of the differences in numerical accuracy. We leave investigation of that to future work. Determination of the effects of different ionosphere conductances on the bubble/blob mechanism will also be left as future work.

Appendix A

[25] To correct equatorial velocity plots for the situation where V_z is nonzero in the equatorial plane, consider two test particles frozen to the same magnetic field line. Particle 1 moves with a fluid element that is crossing the equatorial plane at time t, and particle 2 stays on the same field line as particle 1 but remains at $z = 0$. Both particles are at the same point at time t. Since the two particles remain on the same field line,

$$\mathbf{v}_1 \times \mathbf{B} = \mathbf{v}_2 \times \mathbf{B} \tag{A1}$$

Writing out the three components of (3) and setting $v_{2z} = 0$ gives

$$\mathbf{v}_2 = \mathbf{v} - v_z \frac{\mathbf{B}_e}{B_{ez}} \tag{A2}$$

where $\mathbf{B}_e$ is the magnetic field in the equatorial plane and B_{ez} is its z component. In the above equation, we have written $\mathbf{v}$ instead of $\mathbf{v}_1$, because particle 1 moves with the fluid.

[26] Since $\mathbf{v_2}$ has only x and y components, it is easy to represent in terms of arrow plots in the equatorial plane.

[27] **Acknowledgments.** This work at William Marsh Rice University was supported by National Aeronautics and Space Administration HTP Theory grant NNX08AI55G and National Science Foundation grant ATM-0639772. Work at University of New Hampshire was supported by grant NAS5-02099 (THEMIS) from the National Aeronautics and Space Administration and by grants ATM-0639658, ATM-0902907, and OCI-0749125 from the National Science Foundation.

[28] Masaki Fujimoto thanks Ping Zhu and another reviewer for their assistance in evaluating this paper.

References

Birn, J., M. Hesse, K. Schindler, and S. Zaharia (2009), Role of entropy in magnetotail dynamics, *J. Geophys. Res.*, *114*, A00D03, doi:10.1029/2008JA014015.

Birn, J., R. Nakamura, E. V. Panov, and M. Hesse (2011), Bursty bulk flows and dipolarization in MHD simulations of magnetotail reconnection, *J. Geophys. Res.*, *116*, A01210, doi:10.1029/2010JA016083.

Cattell, C. (1996), Experimental evaluation of the Lundquist number for the Earth's magnetopause and magnetotail, *J. Geophys. Res.*, *101*(A12), 27,309–27,316.

Cheng, C. Z. (2004), Physics of substorm growth phase, onset and dipolarization, *Space Sci. Rev.*, *113*, 207–270, doi:10.1023/B:SPAC.0000042943.59976.0e.

Fuller-Rowell, T. J., D. Rees, S. Quegan, R. J. Moffett, M. V. Codrescu, and G. H. Millward (1996), A coupled thermosphere-ionosphere model (CTIM), in *STEP Handbook on Ionospheric Models*, edited by R. W. Schunk, p. 217, Sci. Comm. on Sol. Terr. Phys., NOAA, Boulder, Colo.

Hu, B., F. R. Toffoletto, R. A. Wolf, S. Sazykin, J. Raeder, D. Larson, and A. Vapirev (2010), One-way coupled OpenGGCM/RCM simulation of the 23 March 2007 substorm event, *J. Geophys. Res.*, *115*, A12205, doi:10.1029/2010JA015360.

Lee, L. C., L. Zhang, G. S. Choe, and H. J. Cai (1995), Formation of a very thin current sheet in the near-Earth magnetotail and the explosive growth phase of substorms, *Geophys. Res. Lett.*, *22*(9), 1137–1140, doi:10.1029/95GL01033.

Lui, A. T. Y. (2004), Potential plasma instabilities for substorm expansion onsets, *Space Sci. Rev.*, *113*, 127–206, doi:10.1023/B:SPAC.0000042942.00362.4e.

Pritchett, P. L. (2007), Onset of magnetic reconnection, in *Reconnection of Magnetic Fields*, edited by J. Birn and E. Priest, pp. 121–132, Cambridge Univ. Press, Cambridge, U. K.

Raeder, J. (2003), Global magnetohydrodynamics—A tutorial, in *Space Plasma Simulation, Lecture Notes in Phys.*, vol. 615, edited by J. Buechner, C. T. Dum, and M. Scholer, pp. 212–246, Springer, Heidelberg, Germany.

Raeder, J., J. Berchem, and M. Ashour-Abdalla (1998), The Geospace Environment Modeling Grand Challenge: Results from a Global Geospace Circulation Model, *J. Geophys. Res.*, *103*(A7), 14,787–14,797, doi:10.1029/98JA00014.

Raeder, J., D. Larson, W. Li, E. L. Kepko, and T. Fuller-Rowell (2008), OpenGGCM simulations for the THEMIS mission, *Space Sci. Rev.*, *141*, 535–555, doi:10.1007/s11214-008-9421-5.

Raeder, J., P. Zhu, Y. Ge, and G. Siscoe (2010), Open Geospace General Circulation Model simulation of a substorm: Axial tail instability and ballooning mode preceding substorm onset, *J. Geophys. Res.*, *115*, A00I16, doi:10.1029/2010JA015876.

Sergeev, V. A., and W. Lennartsson (1988), Plasma sheet at X ≅ −20 RE during steady magnetospheric convection, *Planet. Space Sci.*, *36*, 353–370, doi:10.1016/0032-0633(88)90124-9.

Siscoe, G. L., M. M. Kuznetsova, and J. Raeder (2009), Search for an onset mechanism that operates for both CMEs and substorms, *Ann. Geophys.*, *27*, 3141–3146, doi:10.5194/angeo-27-3141-2009.

Sitnov, M. I., and K. Schindler (2010), Tearing stability of a multiscale magnetotail current sheet, *Geophys. Res. Lett.*, *37*, L08102, doi:10.1029/2010GL042961.

Vasyliunas, V. M. (1975), Theoretical models of magnetic field line merging, *Rev. Geophys.*, *13*(1), 303–336, doi:10.1029/RG013i001p00303.

Wolf, R. A. (1983), The quasi-static (slow-flow) region of the magnetosphere, in *Solar Terrestrial Physics*, edited by R. L. Carovillano, J. M. Forbes, and D. Series, pp. 303–368, D. Reidel, Hingham, Mass.

Wolf, R. A., Y. Wan, X. Xing, J. C. Zhang, and S. Sazykin (2009), Entropy and plasma sheet transport, *J. Geophys. Res.*, *114*, A00D05, doi:10.1029/2009JA014044.

Yang, J., R. A. Wolf, and F. R. Toffoletto (2011), Accelerated thinning of the near-Earth plasma sheet caused by a bubble-blob pair, *Geophys. Res. Lett.*, *38*, L01107, doi:10.1029/2010GL045993.

Zhang, J.-C., R. A. Wolf, S. Sazykin, and F. R. Toffoletto (2008), Injection of a bubble into the inner magnetosphere, *Geophys. Res. Lett.*, *35*, L02110, doi:10.1029/2007GL032048.

Zhu, P., J. Raeder, K. Germaschewski, and C. C. Hegna (2009), Initiation of ballooning instability in the near-Earth plasma sheet prior to the 23 March 2007 THEMIS substorm expansion onset, *Ann. Geophys.*, *27*, 1129–1138, doi:10.5194/angeo-27-1129-2009.

B. Hu, F. R. Toffoletto, R. A. Wolf, and J. Yang, Department of Physics and Astronomy, William Marsh Rice University, Houston, TX 77005, USA. (bh1@rice.edu)

J. Raeder, Space Science Center, University of New Hampshire, Durham, NH 03824, USA.